LASER INTERFEROMETER GRAVITATIONAL WAVE OBSERVATORY
- LIGO -
CALIFORNIA INSTITUTE OF TECHNOLOGY
MASSACHUSETTS INSTITUTE OF TECHNOLOGY

Technical Note	**LIGO-T960042-A - E**	17.05.96

Alignment Tolerances and Re-Alignment Criteria for the LIGO Beam Tubes

Albert Lazzarini

Bill Althouse

Distribution of this draft:

LIGO Science and Engineering

This is an internal working note
of the LIGO Project.

California Institute of Technology
LIGO Project - MS 51-33
Pasadena CA 91125
Phone (818) 395-2129
Fax (818) 304-9834
E-mail: info@ligo.caltech.edu

Massachusetts Institute of Technology
LIGO Project - MS 20B-145
Cambridge, MA 01239
Phone (617) 253-4824
Fax (617) 253-7014
E-mail: info@ligo.mit.edu

WWW: http://www.ligo.caltech.edu/

1 ABSTRACT

This technical note summarizes the dependence of beam tube clear aperture on various sources of misalignment, including fabrication, baffle installations, settlement, and surveying errors.

2 KEYWORDS

Beam tubes, alignment, surveying, tolerances, diffraction noise.

3 OVERVIEW

This technical note summarizes the results of an analysis utilizing the measurements of beam tube out-of-roundness, diameter variation, and deviations from straightness from the CB&I QTR prototypes.

These actual measurements are coupled with a simple mechanical model of beam tube baffle behavior when inserted into the beam tube to produce an estimate of the variability in the geometrical clear aperture from beam tube fabrication and baffle installation.

Additional sources of error are introduced via numerical (Monte Carlo) simulation to model effects of installation misalignment. Two types of misalignment are considered: random, zero-mean fluctuations about a desired value and systematic bias offsets. The former is representative of beam tube shape variations and alignment errors arising from measurement. The latter is representative of long term beam tube settlement, thermal and gravitational deflections, and possible measurement biases in the survey techniques used to bring the beam tube into alignment.

Analytical results have been published by Kip Thorne and Eanna Flanagan which discuss and quantify how the proximity of an optical beam to the edges of the baffles contributes to increased phase noise in a laser interferometer, and how this increased phase noise contributes to strain sensitivity degradation for LIGO. From this work, it is possible to establish a figure of merit with which alignment degradation of the geometrical clear aperture may be quantitatively assessed. From this figure of merit, it is possible to define an *effective clear aperture (D_{eff})* or *noise-equivalent clear aperture (NECA).*

Results are presented which show LIGO strain noise sensitivity to alignment and other errors in terms of clear aperture degradation with increasing misalignment. These results serve to quantify the initial allocation of an alignment error budget and may also be used to determine the need for future re-alignment in terms performance degradation.

4 ESTIMATION OF SOURCES OF ALIGNMENT ERRORS

4.1. CB&I QTR Beam Tube Data

The measurements of beam tube shape used in this analysis were made by CB&I of the two 20m beam tube sections used for the Qualification Test Review (QTR). These tubes, identified as BT#21-3-1 and BT#21-3-2, were measured for straightness, diameter uniformity, and out-of roundness. Using a taut line spanning the length of each tube section, the stand-off distance between the outer beam tube wall and the line was measured every 16” (40.6 cm). Measurements were taken in the middle of the skelp and at the four azimuthal angles 0 , 90 ,180 and 270 . Opposite

pairs of measurements made along the two orthogonal axes (0 - 180 and 90 - 270 data) may be used to obtain average radius, r_0, radius difference, δr, and intersection of the two diameters, (x_c,y_c). The data provide cross section information at 94 points along the 40m length of both tubes (47 points per tube). For each longitudinal location, if an elliptic cross section is assumed, a model of the beam tube profile may be constructed. These are shown in Figure 4-1. Because the data were limited to four measurements, it is not possible to elaborate further on the orientation of the elliptic cross sections or to confirm the validity of the assumption of elliptic cross section. Nonetheless, the degree of uniformity of the measurements indicate that the beam tubes are straight and uniform to a high degree.

Figure 4-1: Reconstructed profiles of the CB&I QTR tube sections. Deviations from a uniform cylinder are amplified 50x in the figure.

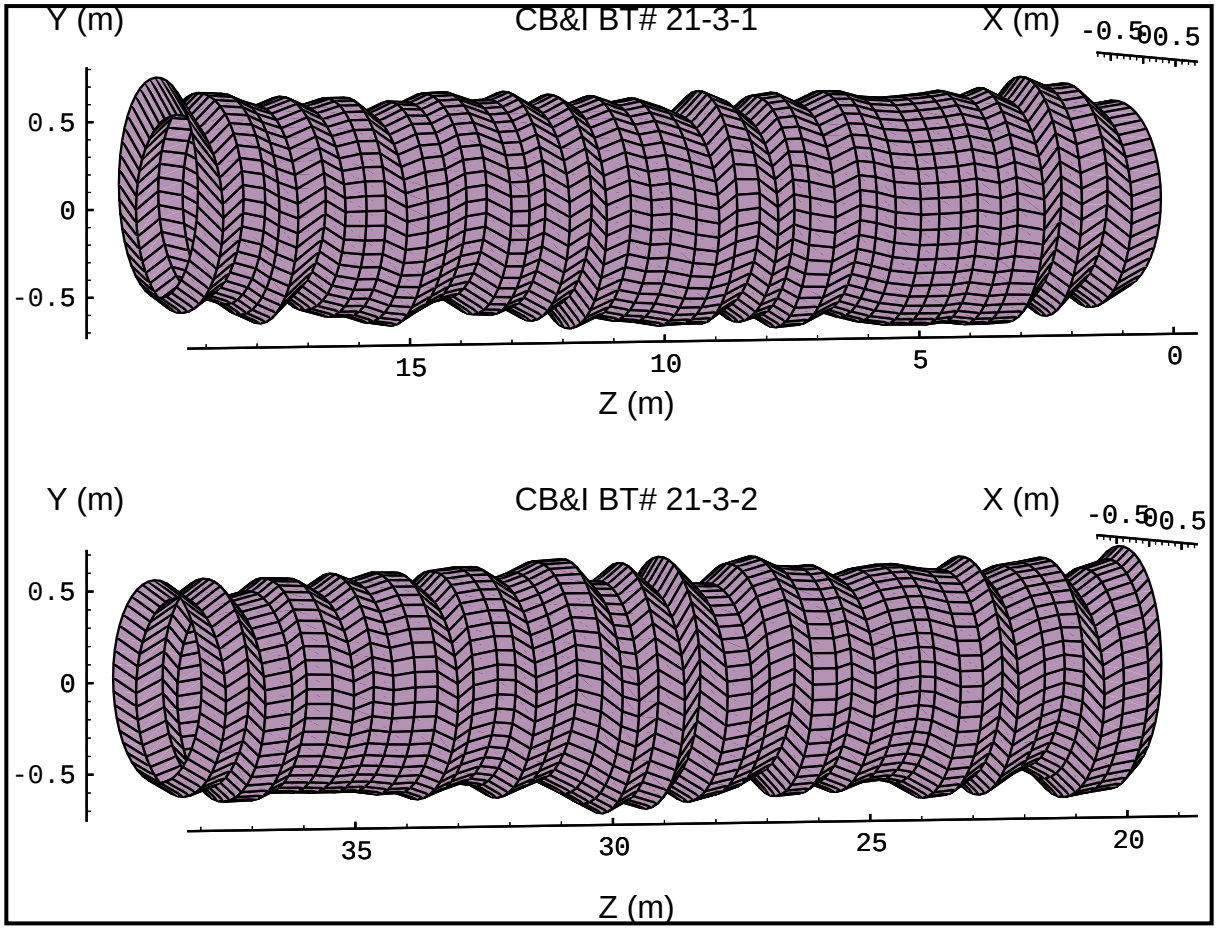

An elliptic model for small excursions from circularity appears justifiable. At each cross section, the average radius and differences between the two x and y diameters was calculated. This set of statistics is described in Table 4-1. The ratios between P-V and σ are not too different from what is expected for a normally distributed random variable (P-V$\approx 5\sigma$ - 6σ).

Table 4-1: Descriptive statistics of the QTR beam tube shape data. Measurements were taken at 4 azimuthal points at 94 longitudinal positions along the combined 40m length of QTR beam tubes CB&I# 21-3-1,2. The effect of skelp and wall thickness variations were included using Monte Carlo methods [<thickness>=3mm; $\sigma_{thickness}$=0.3 mm; **<skelp>=2 mm;** P-V_{skelp}= mm].

Radius		Ellipticity		Centerline	
Average, r_0	0.618 m	Average, Δr	-0.00025 m	$\{x_c, y_c\}$	{0,0}; Defined
σ_r	0.0008 m	$\sigma_{\Delta r}$	0.00051 m	$\{\sigma_{Xc},\sigma_{Yc}\}$	{0.0008 m, 0.0009 m}
Peak-to-Valley	0.0034	Peak-to-Valley	0.0027 m	$\{P\text{-}V_{Xc},P\text{-}V_{Yc}\}$	{.003 m, 0.0054 m}
Ratio of P-V to σ_r	4.0	Ratio of P-V to $\sigma_{\Delta r}$	5.3	Ratios, P-V to σ	{3.7, 5.8}

An end view of the 40 m length of beam tube depicted in Figure 4-1 is shown in Figure 4-2. Figure 4-3 shows the scatter of cross section centers along the combined 40m length of both tubes.

Figure 4-2: End projection of the beam tube wall profiles shown in Figure 4-1. The deviations from average radius are amplified 10x for clarity.

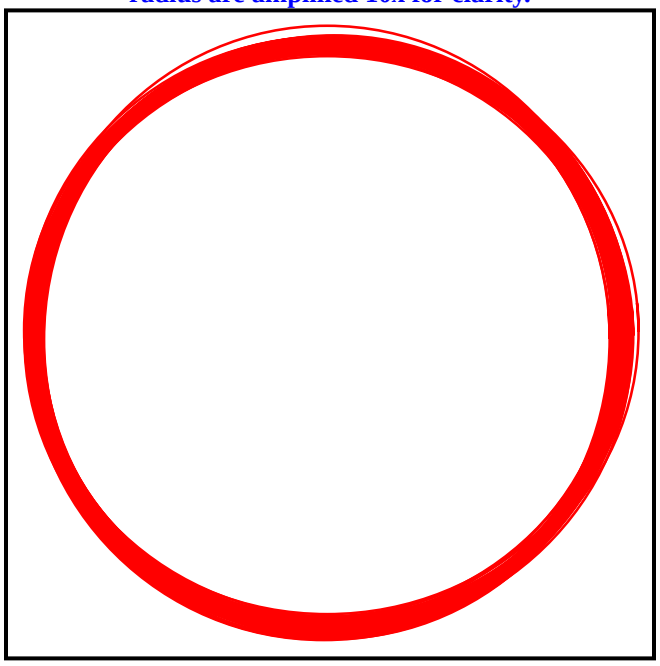

In conclusion, the QTR data indicate the beam tubes are straight and exhibit small deviations from a uniform circular cross section. There are additional effects and sources of fabrication error which are not accounted for in the QTR data. These include:

1. Measurements at 0 and 180 , and 90 and 270 were individually taken with a longitudinal offset of 1/4 skelp width or approximately 10 cm relative to each other. However, the measurements were assumed to lie in a plane normal to the beam tube centerline in the analysis.

2. The scalloping of the beam tube due to weld shrinkage modulates the beam tube inner diameter. This effect is concentrated near the spiral weld, and is crossed once by each

baffle at an arbitrary azimuthal position. Measurement of the scalloping after the QTR indicate the magnitude of the effect is 0.002 m. This effect was included in modeling the baffle edge locations (see note in Table 4-1 and also below).

Figure 4-3: Distribution of beam tube centerlines measured at 94 points over 40m. Histograms are frequency of occurrence along x and y axes.

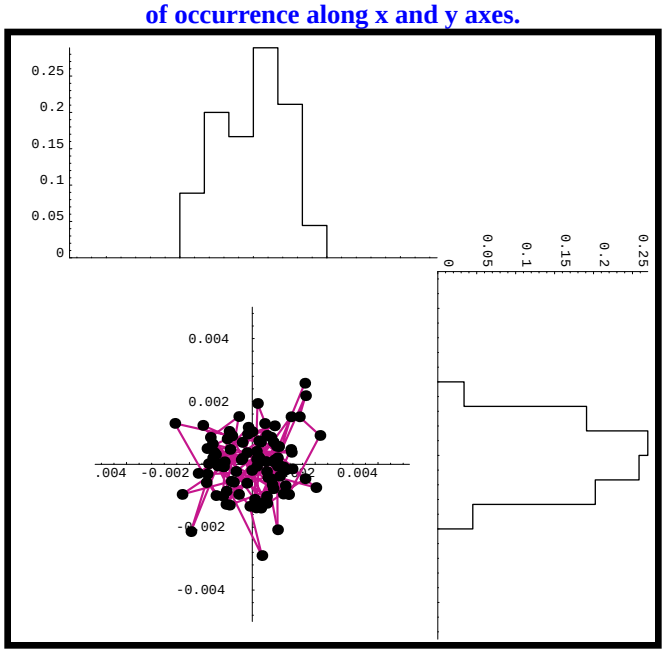

3. Since circumference data were not taken, it is not possible to estimate the error in assuming the diametric measurements may be modeled by an ellipse oriented with major and minor axes along the 0 /180 and 90 /270 lines. Infrequent measurements of circumference which are available indicate that this assumption appears reasonable.

4. Measurements were taken on the outer diameter of the beam tubes; thickness variations in the stock material were not measured at the same time.The nominal thickness and a small variation in thickness was included in modeling the baffle inner edge locations (see note in Table 4-1 and also below).

5. The installed beam tubes are aligned relative to a stiffening ring welded to the outside of the tube. A loose fit between stiffener and beam tube would cause an eccentricity between them. CB&I has allocated an inner diameter tolerance of +/- .75 mm and an outer diameter tolerance of +/- .5 mm.

6. Gravitational sag of the beam tube. The tube was rotated so that all measurements were performed along a line in the horizontal plane (e.g., either the 3:00 o'clock or 9:00 o'clock positions). The magnitude of this effect is predicted to be -0.00125 m (L. Jones, calculation) and is maximum near the mid-point of a 20m section of tube. Differences between fixed and sliding supports cause the point to be slightly closer to the sliding support.

7. Thermal gradients along the vertical within the beam tube enclosure will cause the tube to

deform. This effect is estimated to be a maximum of +0.00225 m (D. Coyne and L. Jones, calculation). The effect is approximately 2x the effect due to gravity and in the opposite sense. Taken together, the net deflection of the tube is *upwards* +0.001 m at roughly the midpoint between supports.

4.2. BEHAVIOR OF BAFFLES WITHIN BEAM TUBE

The mechanical design of the baffle is depicted in Figure 4-4. It consists of a cylindrical band which conforms to the inner diameter of the tube and a conical section (frustum) which projects into the beam tube aperture. The inner edge of the baffle defines the clear aperture of the tube. The conical frustrate makes an angle of 35 with the cylinder and projects radially 0.09 m into the beam tube.

Figure 4-4: 3D model of a beam tube baffle.

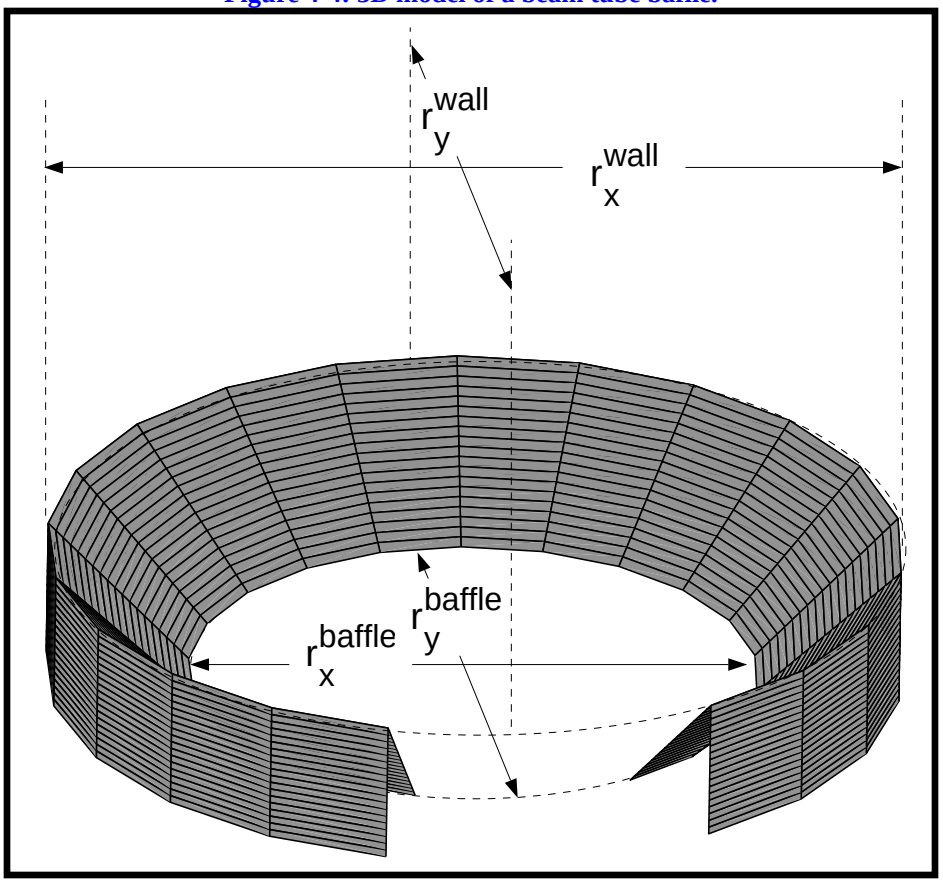

Diameter (scale) changes

The geometry of the assembly is such that a change in radius of the band affects the angle and thus the projection into the beam tube. By considering a change of tube diameter, the relationship between change of baffle edge radius and tube diameter is given by:

$$\delta r^{baffle} = \delta r^{wall} \frac{r^{baffle}}{r^{wall}} \qquad [1]$$

Elliptic deformations (area-preserving)

If the tube is deformed elliptically, the baffle deforms with an azimuthal dependence which amplifies the deformation at its outer edge:

$$\delta(r[\theta])^{baffle} = -3\delta r^{wall}\left(\frac{r^{baffle}}{r^{wall}}\right)\cos 2\theta \qquad [2]$$

Appendix 1 provides the derivation. This shows that deviations in the shape of the beam tube are amplified at the inner edge of the baffles. Figure 4-5 shows this effect. A numerical finite element analysis (FEA) for the baffle design shown above gives an amplification factor of approximately 2x instead of 3x. For the analysis performed here, the more conservative factor 3x has been used.

Figure 4-5: Depiction of the relationship between tube wall deformation and the inner edge of the baffle according to the model in Eq. [4].

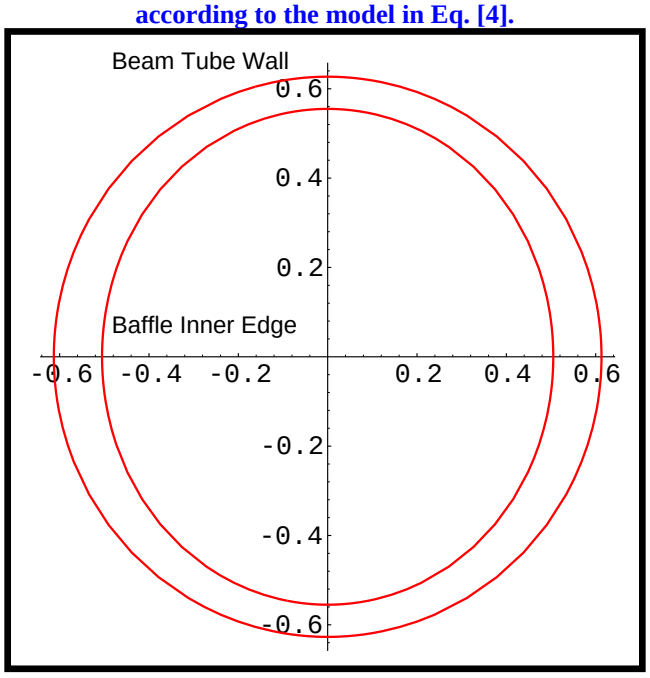

In going from QTR measured data to the baffle inner edge, the following effects were modeled and included:

1. The scalloping of the skelp between the sprial weld introduces a raised ridge within the beam tube approximately 2 mm high. This welt is localized at the point where the cylindrical portion of the baffle crosses the spiral weld, which will occur once per baffle. The effect of the scalloping is modeled as a reduction of the inner radius of the beam tube by a uniform random variable with mean of 2 mm, with a peak-to-valley of 1 mm. This reduction is randomly distributed in azimuth and affects the major and minor axes of the elliptic cross section proportionately. The net effect is to reduce the elliptical radii and also to introduce an offset in the aperture center with respect to the bare tube wall.

2. The beam tube is nominally 0.125” thick (3 mm). A normal variate with standard deviation of 10% about this average value was also included. This effect affects centering of the

cross section and also reduces the inner radii of the cross section.

3. The baffle response to being conformed to an elliptic inner tube cross section was modeled as described above.

Figure 4-6 depicts an end projection of an ensemble of baffles which are located at each of the beam tube cross sections where QTR data are available. Also indicated in the figure is the design 1 m geometric clear aperture, locations of two interferometer beams for the initial LIGO configuration (Hanford system, near tube center) and a beam located at the extreme periphery of the 1 m clear aperture.

Figure 4-6: End-on view of the beam tube with baffles in place.

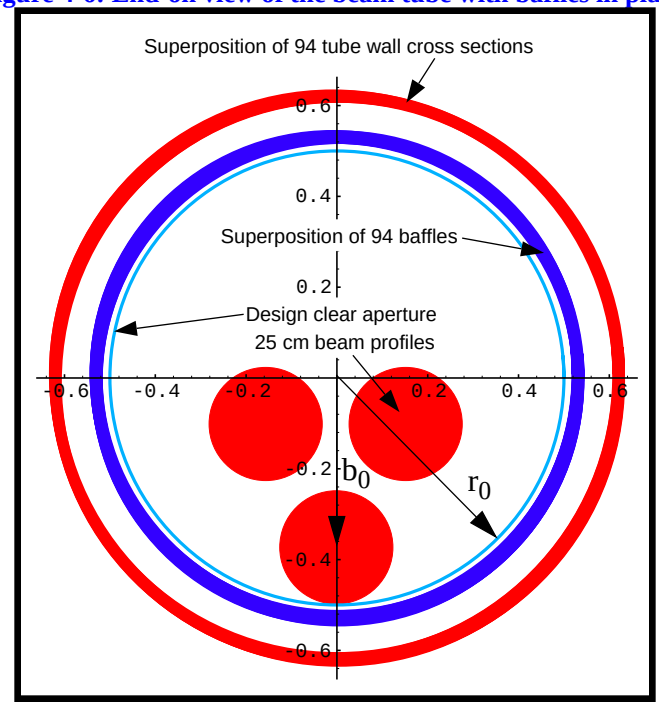

Figure 4-7 shows the distribution in distances from the beam tube center to the inner edge of the baffles. The distribution is a Monte Carlo simulation. For the 94 baffles located at each of the measured beam tube cross sections, 30 random points distributed uniformly in azimuth were sampled. This ensemble of distances was then used in the subsequent statistical analysis.

Figure 4-7: Distribution of distances from beam tube center to the inner edge of the baffles. Statistical descriptors are listed in Table 4-2.

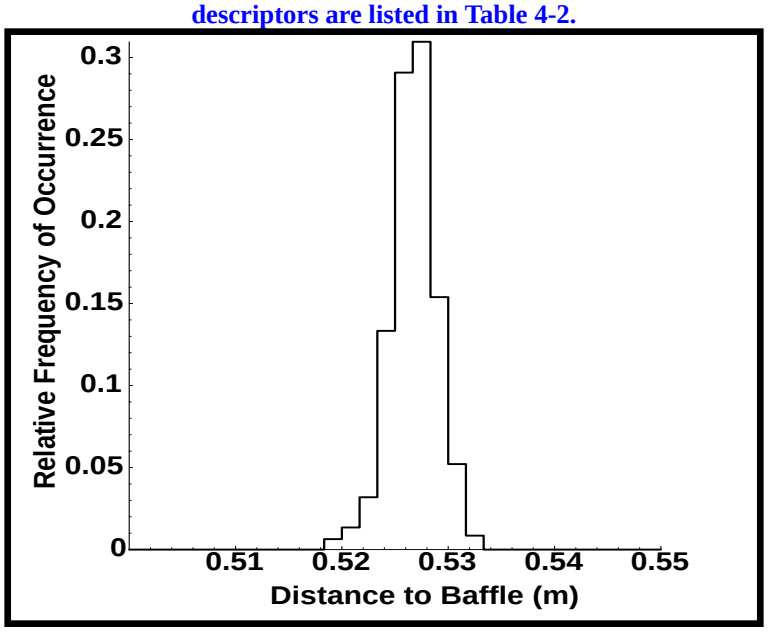

Table 4-2: Descriptive statistics of the inner edge of an ensemble of baffles inserted at each of the measured cross sections of the QTR tube. Compare to Table 4-1. Approximate effects of skelp, tube wall thickness, and centering ring eccentricity on the baffle seating within the inner beam tube wall were incorporated in the simulation (see text and Table 4-1).

Inner Radius		Aperture Ellipticity		Aperture Centerline	
Average, r_0	0.527 m	Average, Δr	-0.0003 m	$\{x_c,y_c\}$	{0.00003 m, 0.000035 m}
σ_r	0.002 m	$\sigma_{\Delta r}$	0.0006 m	$\{\sigma_{Xc}, \sigma_{Yc}\}$	{0.0009 m, 0.001 m}
Peak-to-Valley	.009	Peak-to-Valley	0.0033 m	$\{P\text{-}V_{Xc},P\text{-}V_{Yc}\}$	{0.004 m, 0.005 m}
Ratio of P-V to σ_r	5.1	Ratio of P-V to $\sigma_{\Delta r}$	5.5	Ratios, P-V to σ	{4.4, 5.3}

4.3. EFFECT ON INTERFEROMETER OPTICAL PERFORMANCE: NOISE EQUIVALENT CLEAR APERTURE

Thorne and Flanagan have shown (LIGO-T950045-00-E) that the worst-case diffraction noise for LIGO will occur for optical beams located near the periphery of the clear aperture. Figure 4-6 shows the beam tube with an extreme off-axis beam located at the bottom of the clear aperture.

In particular, it is possible to define a *noise equivalent clear aperture (NECA)* by considering the increase in diffraction noise relative to an ideal clear aperture. This is done by expanding the factor responsible for increased diffraction noise in off-axis beams to second order in small deviations which bring the optical beam closer to the baffle edges. Appendix 2 discusses how variations in baffle edge height can be incorporated into the diffraction model of T950045. Using expansion [B.5] one has:

$$r_{eff} \sim r_0 - \delta - \frac{7}{2}\frac{\sigma^2}{(r_0 - b_0)} + \ldots \qquad [3]$$

Expression [3] is compared to the results of Monte Carlo simulations in Figure 4-8.

Figure 4-9 presents the three dimensional surface for simultaneous variations in both bias and random errors. The 1m noise equivalent clear aperture is indicated.

Figure 4-8: Dependence of the noise equivalent clear aperture on bias and random errors. For small errors of a magnitude of interest to LIGO, the analytical expression accurately reproduces the degradation. The types of errors considered are shown schematically.

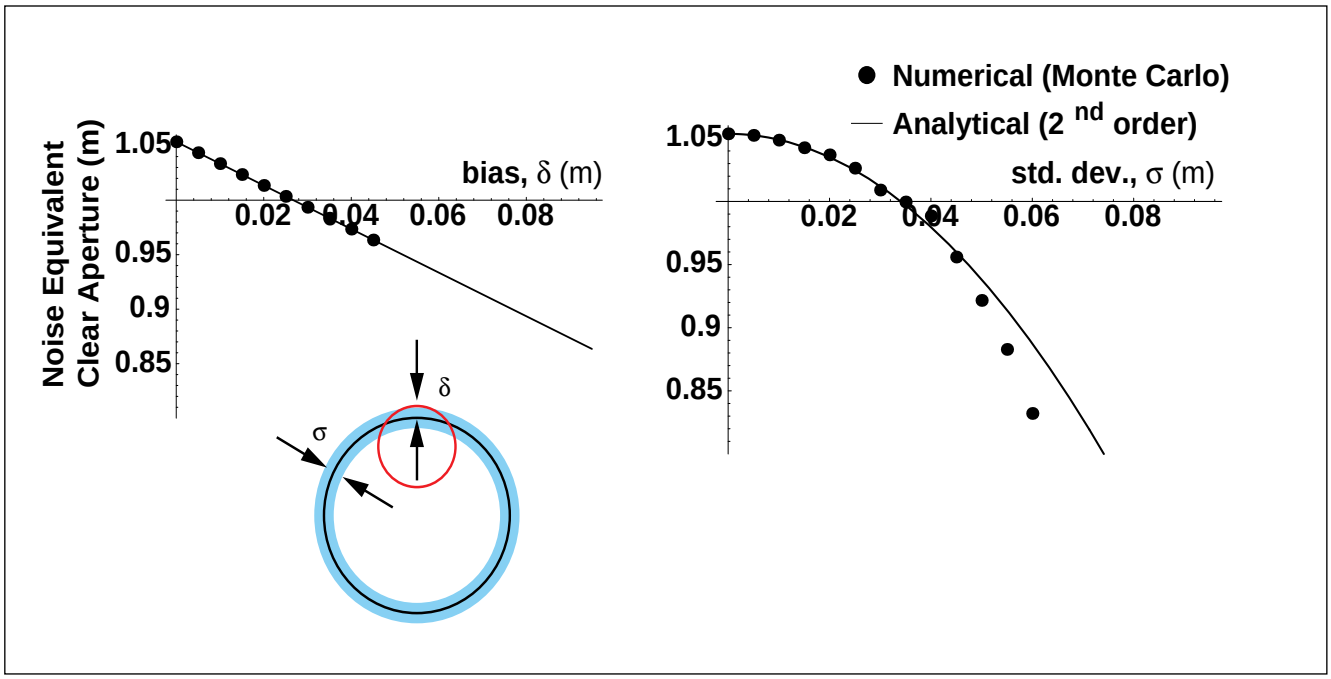

Figure 4-9: Contours of constant noise equivalent clear aperture

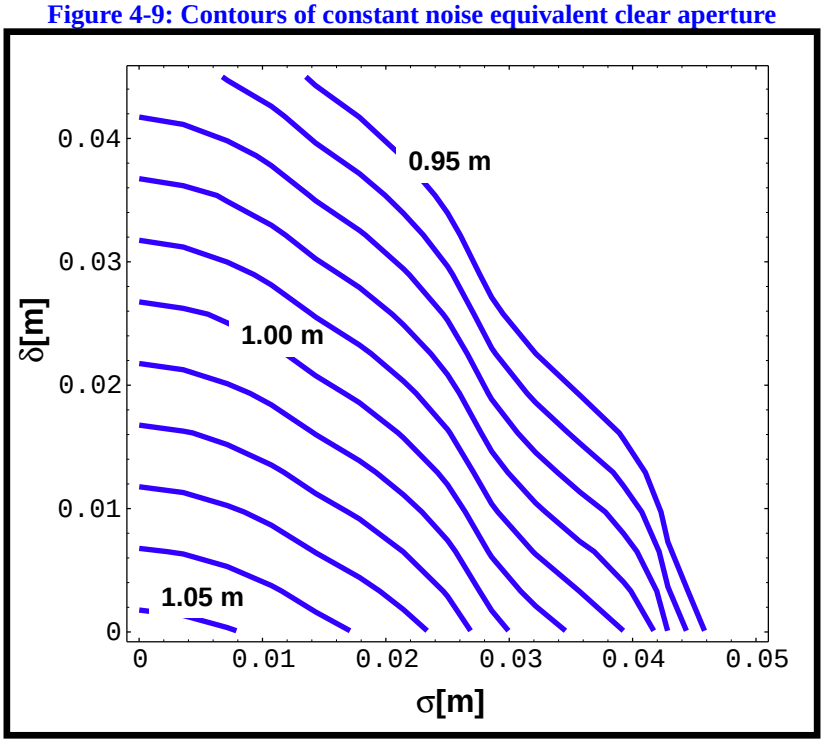

5 CONCLUSIONS

Using the effect on diffraction and phase noise derived by Thorne and Flanagan, it is possible to develop a quantitative definition for a noise equivalent clear aperture. Using the best information available at present and assuming CB&I will be able to reproduce the QTR results, the effective clear of the beam tubes with baffles inserted is expected to start out slightly larger then 1.05 m. Alignment errors during installation and later slab settlement will cause the effective clear aperture to be degraded from this maximum value.

Degradation of the initial clear aperture with the introduction of bias is linear with a 1:1 effect on clear aperture. On the other hand, degradation caused by randomly distributed errors is more benign, affecting the noise equivalent clear aperture only in second order for small errors:

$$\left.\frac{r_{eff}-r_0}{r_0}\right|_{\text{constant }\delta} = \frac{\delta r}{r_0} = -\frac{7}{2}\frac{\sigma^2}{r_0(r_0-b_0)} \approx -0.0056\sigma^2(\text{in cm}^2)\ ;\ r_0 = 50\text{cm}, b_0 = 37.5\text{cm} \qquad [4]$$

A random error of σ=1 cm reduces the effective clear aperture by 0.6% or 0.6 cm on a 1 m diameter.

Starting with a tube of the quality represented by the QTR sections, the LIGO requirement of a 1 m clear aperture allows *either* up to 2.7 cm of bias or 3.5 cm of random error to be introduced during the installation and alignment. The 1 m contour of Figure 4-8 indicates the trade-off which can be made between these types of errors. This will be useful during construction as a predictive tool to allocate the total error between the two types of error. Later, during operations, the contour allows one to make a trade-off between re-alignment and continued operation at a degraded value of effective clear aperture.

APPENDIX 1 BAFFLE DEFORMATION INSIDE AN ELLIPTIC TUBE

If the tube is deformed elliptically, the baffle deforms with an azimuthal dependence which amplifies the deformation of its outer edge. This may be understood by assuming that the cylindrical band at the outer edge of the baffle conforms locally to the radius of curvature of the tube wall. In the expression above, δr_{tube} corresponds to the change in the local radius of curvature of the cylinder. For an ellipse defined by

$$\frac{x^2}{r_x^2} + \frac{y^2}{r_y^2} = 1 \qquad [A.1]$$

The radius of curvature is given by

$$|\rho(x)| = \frac{r_x^2}{r_y}\left(1 + \frac{x^2}{r_x^2}\left(\frac{r_y^2}{r_x^2} - 1\right)\right)^{\frac{3}{2}} \qquad [A.2]$$

For small deviations from a circle, $r_x=r_0-\delta r$, $r_y=r_0+\delta r$, $x=r_0\cos\theta$. Expansion of equation [A.2] to first order in δr gives:

$$\delta\rho[\theta] = 3\delta r \cos 2\theta \qquad [A.3]$$

Substitution of [A.3] into [1] gives:

$$\delta(r[\theta])^{baffle} = \delta\rho[\theta]\left(\frac{r^{baffle}}{r^{wall}}\right) = 3\delta r^{wall}\left(\frac{r^{baffle}}{r^{wall}}\right)\cos 2\theta \qquad [A.4]$$

APPENDIX 2 NOISE EQUIVALENT CLEAR APERTURE

Thorne and Flanagan have shown (LIGO-T950045-00-E) that the worst-case diffraction noise for LIGO will occur for optical beams located near the periphery of the clear aperture.

The excess phase noise due to diffraction caused by the proximity of a beam to the edge of the clear aperture is given by:

$$h^2[f]_{diff} \sim \left(\frac{1}{r_0 - b_0}\right)^6 \qquad [B.1]$$

The variables shown in Figure 4-6 are used. The distribution of distances about the average distance from beam tube center to the tops of the baffles can be characterized by a zero mean random variable, $r=r_0+\varepsilon$. Figure 4-7 shows that this is an valid assumption. In addition to fabrication errors, there will also be installation and alignment errors. Any systematic offset of beam tube center with respect to the optical beam center may be represented by a bias term, $b = b_0 + \delta$. Such contributions are expected to come from gravitational sag, thermal distortion, and possibly measurement bias in the alignment process.

In the presence of both alignment and fabrication errors, the net effect from an ensemble of many baffles on the diffraction phase noise is determined by taking the ensemble average over the baffle distribution:

$$\tilde{h}[f]_{diff} = \langle h^2[f]_{diff} \rangle^{\frac{1}{2}} \sim \left\langle \left(\frac{1}{(r_0 + \varepsilon) - (b_0 + \delta)} \right)^6 \right\rangle^{\frac{1}{2}} \qquad [B.2]$$

Assuming ε/r_0, $\delta/b_0 << 1$, and $<\varepsilon>=0$; $<\varepsilon^2> = \sigma^2$, $<\delta> = \delta$ and $<\delta^2>-<\delta>^2 = 0$, the Taylor series expansion to second order in ε and δ becomes:

$$\tilde{h}[f]_{diff} \sim \left(\frac{1}{r_0 - b_0} \right)^3 \left(1 + 3\frac{\delta}{r_0 - b_0} + \frac{21}{2}\frac{\sigma^2}{(r_0 - b_0)^2} + \frac{6\delta^2}{(r_0 - b_0)^2} \right) \qquad [B.3]$$

It is possible to define a *noise equivalent clear aperture* by considering equations B.1 and B.3:

$$(\tilde{h}[f]_{diff}) \sim \left(\frac{1}{r_{eff} - b_0} \right)^3 \quad ; \quad r_{eff} \sim \left(\frac{b_0 \, \tilde{h}[f]_{diff}^{\frac{1}{3}} + 1}{\tilde{h}[f]_{diff}^{\frac{1}{3}}} \right) \qquad [B.4]$$

Substituting expansion B.3 For $\tilde{h}[f]_{diff}$, one obtains:

$$r_{eff} \sim r_0 - \delta - \frac{7}{2}\frac{\sigma^2}{(r_0 - b_0)} + \ldots \qquad [B.5]$$